

## **$\alpha$ -Synuclein-Induced Membrane Remodeling Is Driven by Binding Affinity, Partition Depth, and Interleaflet Order Asymmetry**

Anthony R. Braun,<sup>†</sup> Michael M. Lacy,<sup>‡</sup> Vanessa C. Ducas,<sup>§</sup> Elizabeth Rhoades,<sup>‡</sup> and Jonathan N. Sachs\*,<sup>†</sup>

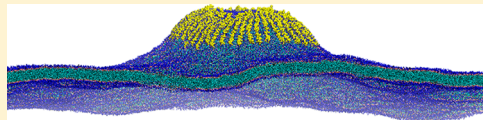
<sup>†</sup>Department of Biomedical Engineering, University of Minnesota, Minneapolis, Minnesota 55455, United States

<sup>‡</sup>Department of Molecular Biophysics and Biochemistry, Yale University, New Haven, Connecticut 06520, United States

<sup>§</sup>Department of Pediatrics, Yale School of Medicine, New Haven, Connecticut 06520, United States

### **S Supporting Information**

**ABSTRACT:** We have investigated the membrane remodeling capacity of the N-terminal membrane-binding domain of  $\alpha$ -synuclein ( $\alpha$ -Syn<sub>100</sub>). Using fluorescence correlation spectroscopy and vesicle clearance assays, we show that  $\alpha$ -Syn<sub>100</sub> fully tubulates POPG vesicles, the first demonstration that the amphipathic helix on its own is capable of this effect. We also show that at equal density of membrane-bound protein,  $\alpha$ -Syn has dramatically reduced affinity for, and does not tubulate, vesicles composed of a 1:1 POPG:POPC mixture. Coarse-grained molecular dynamics simulations suggested that the difference between the pure POPG and mixture results may be attributed to differences in the protein's partition depth, the membrane's hydrophobic thickness, and disruption of acyl chain order. To explore the importance of these attributes compared with the role of the reduced binding energy, we created an  $\alpha$ -Syn<sub>100</sub> variant in which we removed the hydrophobic core of the non-amyloid component (NAC) domain and tested its impact on pure POPG vesicles. We observed a substantial reduction in binding affinity and tubulation, and simulations of the NAC-null protein suggested that the reduced binding energy increases the protein mobility on the bilayer surface, likely impacting the protein's ability to assemble into organized pretubule structures. We also used simulations to explore a potential role for interleaflet coupling as an additional driving force for tubulation. We conclude that symmetry across the leaflets in the tubulated state maximizes the interaction energy of the two leaflets and relieves the strain induced by the hydrophobic void beneath the amphipathic helix.



$\alpha$ -Synuclein ( $\alpha$ -Syn) is a 140 amino acid, intrinsically disordered neuronal protein whose N-terminal domain (residues 1–93) adopts an amphipathic helix (AH) upon binding to membranes.<sup>1–5</sup> It is well-established that full-length  $\alpha$ -Syn is capable of dramatic remodeling of lipid bilayers. *In vivo*,  $\alpha$ -Syn has recently been shown to induce mitochondrial fragmentation and fission.<sup>6,7</sup> *In vitro*, biophysical experiments have shown that  $\alpha$ -Syn induces externally protruding membrane tubules from synthetic lipid vesicles and can cause full fragmentation at high enough protein concentrations.<sup>8,9</sup> Combining X-ray scattering with coarse-grained molecular dynamics (CGMD) simulations, we have recently shown that  $\alpha$ -Syn thins membranes and induces complex curvature fields.<sup>10</sup> In general, amphipathic helices like that of  $\alpha$ -Syn can both sense and induce curvature upon binding a membrane,<sup>3,8,10–18</sup> and the biophysical mechanisms by which they do so have been widely studied.<sup>16,19–32</sup> The 47 C-terminal residues of  $\alpha$ -Syn are known to remain disordered upon binding of the AH,<sup>3–5,33,34</sup> but whether these residues are necessary for tubulation has not been established. Similarly, a potential role of the important hydrophobic non-amyloid component (NAC) domain (best known for its role in protein aggregation) in tubulation has not been explored in the context of the full membrane-binding domain.<sup>35</sup>

At high concentrations,  $\alpha$ -Syn causes complete tubulation and fragmentation of negatively charged 1-palmitoyl-2-oleoyl-*sn*-glycero-3-phosphoglycerol (POPG) giant unilamellar

vesicles (GUVs) but has a negligible effect on neutral 1-palmitoyl-2-oleoyl-*sn*-glycero-3-phosphocholine (POPC) GUVs.<sup>8</sup> This difference is attributed to a very low binding affinity of  $\alpha$ -Syn for POPC lipids.<sup>14</sup> Less aggressive tubulation (compared with pure POPG bilayers) has also been observed in vesicles with a mixed anionic and zwitterionic lipid composition [e.g., POPG:POPC, POPG:1-palmitoyl-2-oleoyl-*sn*-glycero-3-phosphoethanolamine (POPE), or 1-palmitoyl-2-oleoyl-*sn*-glycero-3-phosphate (POPA):POPC].<sup>8,9</sup> This finding, however, is considerably more provocative because, unlike in the case of POPC, the cause of reduced tubulation has not been attributed to reduced binding affinity.

We previously used fluorescence correlation spectroscopy (FCS) to show that in 1:1 1-palmitoyl-2-oleoyl-*sn*-glycero-3-phosphoserine (POPS):POPC vesicles, the  $\alpha$ -Syn binding site is made up of ~20 lipids (~40 lipids if one includes both leaflets). Furthermore, we showed that the size of this binding site is independent of  $K_D$  and vesicle size.<sup>14</sup> Our experimentally measured value of ~20 lipids per bound  $\alpha$ -Syn corresponds very well with the number of lipids required to accommodate an extended  $\alpha$ -helical  $\alpha$ -Syn on the bilayer, consistent with our recent all-atom and CGMD calculations.<sup>10,15</sup> Thus, it has been reasonably concluded that at very high concentrations of bound protein, the membrane surface area—not the lipid charge or

Received: February 18, 2014

Published: June 24, 2014



number of defects—limits the density of  $\alpha$ -Syn at saturation. Therefore, on the basis of measured  $K_D$  values, equal and saturating surface density of  $\alpha$ -Syn can be achieved in purely anionic lipids or 1:1 mixtures by adjusting the amount of protein added to solution for each lipid composition.<sup>14</sup>

While previous  $\alpha$ -Syn tubulation studies were done at extremely high protein concentrations, they did not account for potential differences between the  $K_D$  values for pure POPG and POPG:POPC (PG:PC) mixtures.<sup>8,9</sup> This presents a complication in confidently elucidating the sources of the reduction in tubulation propensity in the mixture, which may simply be attributed to a subthreshold density of protein bound to the vesicle surface. As recently discussed, simply immersing a vesicle in a protein solution does not result in membrane-bound protein concentrations equal to the protein concentration in bulk.<sup>36</sup> Indeed, we will show a striking reduction in  $\alpha$ -Syn's apparent binding affinity for the lipid mixture under dilute conditions.<sup>18,36</sup> It was therefore absolutely essential that we design our tubulation experiments under conditions where an equal amount of  $\alpha$ -Syn was bound regardless of vesicle composition.

As will be elaborated throughout, theory and simulations have recently emphasized the importance of (1) protein insertion depth in dictating curvature induction<sup>29</sup> and (2) binding energy in promoting protein organization, curvature, and membrane disruption.<sup>20,37</sup> In that context, in the present study we have first demonstrated that the C-terminal residues of  $\alpha$ -Syn are not necessary for tubulation, showing instead that tubulation can be achieved solely by the membrane-bound AH. Second, we have confirmed that the reduction of  $\alpha$ -Syn-induced tubulation of 1:1 PG:PC bilayers, compared with pure POPG bilayers, can be attributed to differences in the protein's interaction with the lipid matrix (including depth of partition and mobility) and not dismissed as a consequence of a subthreshold density of bound protein. Third, we have investigated the role of the NAC domain on binding affinity and tubulation by engineering an  $\alpha$ -Syn variant lacking the hydrophobic core of the domain (NAC-null).

We then used CGMD simulations in an effort to correlate the macroscopic experimental observation (tubulation) with molecular-scale perturbations of the membrane and protein mobility. Although CGMD simulations may lack the detail and sampling to definitively explain our experimental findings, these models do provide insight that can guide speculation regarding the relative roles of protein partition depth and binding energy.<sup>10</sup> In the context of an already rich simulation literature regarding protein-induced membrane remodeling,<sup>10,15,19,22,37–43</sup> we have asked the following questions: What differences in the lipid behavior are observable when  $\alpha$ -Syn is bound to a pure POPG bilayer as compared with a 1:1 PG:PC mixture? Also, are there observable differences between wild-type and NAC-null  $\alpha$ -Syn that can shed light on the mechanism of tubulation? Our experimental results, supported by our simulations, provide strong support for the importance of both binding energy and partition depth, as has been recently emphasized.<sup>20,29,37</sup> We also highlight a new finding regarding lipid chain order as a potential additional driving force for tubulation.

All of the experiments and simulations involved the 100 N-terminal residues of either  $\alpha$ -Syn ( $\alpha$ -Syn<sub>100</sub>) or of designed  $\alpha$ -Syn variants. For 100% POPG and 1:1 PG:PC vesicles, the  $\alpha$ -Syn<sub>100</sub> binding affinity was assayed with FCS. Then bound protein was equalized by adjusting for measured  $K_D$  values, and

vesicle clearance assays were performed to monitor  $\alpha$ -Syn<sub>100</sub>-induced membrane remodeling.<sup>8</sup> Simulations studies were performed on the membrane-bound helical form of the protein. We used the GROMACS v4.5.3 simulation package<sup>44,45</sup> and the MARTINI<sup>46,47</sup> CGMD force field. Simulations were performed in the isothermal-isobaric (constant temperature and pressure, *NPT*) ensemble (1 bar and 303 K, respectively) with the *xy* and *z* dimensions semi-isotropically coupled to independent barostats, resulting in a tensionless membrane.<sup>48</sup> Membrane tubulation by  $\alpha$ -Syn<sub>100</sub> is a complex process that involves binding, folding, partitioning, and membrane remodeling events, each with its own energetic barrier and kinetic threshold. The MARTINI force field requires a predefined protein secondary structure, precluding the simulation of both the binding and folding stages. Nevertheless, our previous  $\alpha$ -Syn<sub>100</sub> study using the MARTINI force field demonstrated good agreement with our experimental X-ray measurements of  $\alpha$ -Syn<sub>100</sub>-induced membrane remodeling.<sup>10</sup>

We simulated a total of 18 systems: four pure lipid systems (POPC, 1:3 PG:PC, 1:1 PG:PC, and POPG), each with 3200 lipids, 70 400 CG waters, and counterions; eight low-density  $\alpha$ -Syn<sub>100</sub> systems, each with 3200 lipids, two proteins, 70 400 CG waters, and counterions; three high-density (~400:1 lipid:protein) systems, each with 3016 lipids and eight proteins; and three tubule-nucleation systems, each with 85 296 lipids, 48 proteins, 3 996 000 CG waters, and counterions. The  $\alpha$ -Syn<sub>100</sub> protein was modeled as an extended helix with residues 1–93 as  $\alpha$ -helical and residues 94–100 as a random coil.<sup>10</sup> Full details of the simulation run parameters and system construction are presented in the Supporting Information (SI). The 14 small systems were simulated for a total of 12  $\mu$ s (actual simulation time), with the last 5  $\mu$ s used for analysis. For the 12 low-density (1600:1 lipid:protein) systems, the two  $\alpha$ -Syn<sub>100</sub> proteins were positioned on opposite leaflets in remote regions of the membrane, ensuring a globally symmetric system without any a priori global area mismatch between the two leaflets while removing competing transverse protein–protein interactions (see Supplemental Figure 1C). The ~85 000-lipid systems were constructed to explore  $\alpha$ -Syn<sub>100</sub>-induced tubule nucleation. Instead of using a free-floating membrane—where tubulation is the result of protein rolling up a floppy bilayer—we started with a periodically coupled, flat bilayer and introduced three different protein structures, each with 48  $\alpha$ -Syn<sub>100</sub> that were arranged radially (“spoke” geometry), in concentric circles (“circumferential” geometry), or as a linear arrayed patch (“carpet” geometry). We removed 23 lipids per protein from the protein monolayer to minimize the global area mismatch, an approach we have used previously.<sup>10</sup> The rationale for how we designed the various systems will be discussed in the context of how our findings complement and advance existing understanding of AH-induced membrane remodeling.<sup>10</sup>

## RESULTS

**Headgroup Charge Density Dictates Tubulation Capacity.** FCS was used to determine the relative affinity of  $\alpha$ -Syn<sub>100</sub> for large unilamellar vesicles (LUVs) composed of 100% POPG or 1:1 (mol/mol) PG:PC under dilute conditions. Binding of fluorescently labeled protein to unlabeled vesicles results in a shift in the autocorrelation curves to the right (longer diffusion times) (Figure 1A); the autocorrelation curves can then be fit to extract the fraction of bound protein and to determine an apparent binding affinity,  $K_D$  (see Materials and Methods in the SI for details). These measurements found that

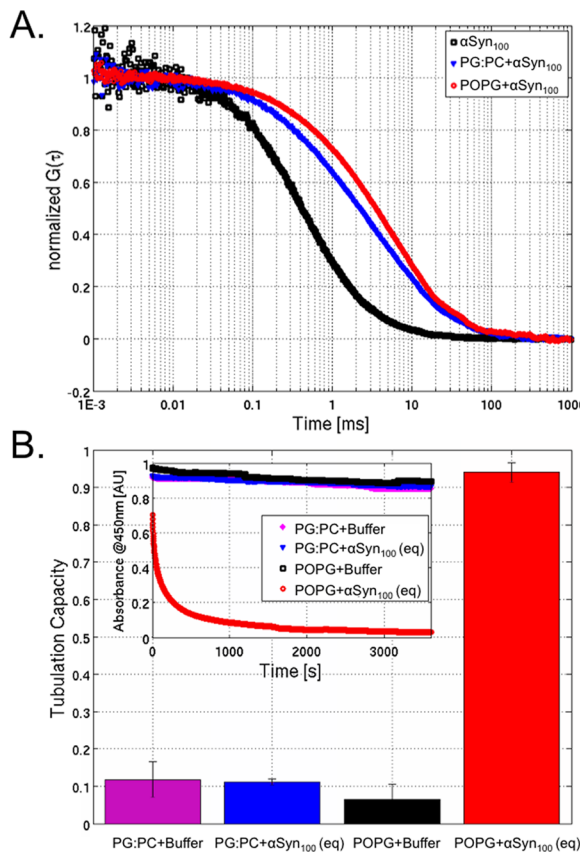


**Figure 1.** (A) FCS traces for  $\alpha\text{-Syn}_{100}$  in the absence (black) or presence of equal concentrations of 1:1 PG:PC (blue) or 100% POPG (red) LUVs. The greater shift to the right in the 100% POPG curve reflects a larger fraction of  $\alpha\text{-Syn}_{100}$  bound relative to the 1:1 PG:PC curve. (B)  $\alpha\text{-Syn}_{100}$  tubulation capacities for 1:1 PG:PC and 100% POPG at equal bound density, compared with buffer. The inset shows the corresponding absorbance traces for systems with 1:1 PG:PC or 100% POPG and buffer or  $\alpha\text{-Syn}_{100}$ .

$\alpha\text{-Syn}_{100}$  binds to 100% POPG vesicles with  $\sim$ 60 times greater affinity than to 1:1 PG:PC vesicles ( $K_D = 2.25$  and  $136.9 \mu\text{M}$ , respectively) under our buffer conditions. This result agrees with previous studies showing that  $\alpha\text{-Syn}_{100}$  binding to lipids is driven primarily by electrostatic interactions between anionic lipid headgroups and positively charged lysine residues in the membrane-binding region of the protein,<sup>14,49–51</sup> although the complex roles of hydrophobic lipid–protein interactions and entropy cannot be ruled out.

In order to test the effect of headgroup charge on  $\alpha\text{-Syn}_{100}$ -induced tubulation at equal bound-protein density, we adjusted the added protein concentration on the basis of the measured  $K_D$  value. Again, because of our previous measurements under saturating conditions, this ensured equal density of bound protein.<sup>14</sup> The ability of  $\alpha\text{-Syn}_{100}$  to tubulate liposomes was assayed by monitoring the change in the amount of scattered light from a liposome solution in the presence of  $\alpha\text{-Syn}_{100}$ .<sup>8</sup> We quantified  $\alpha\text{-Syn}_{100}$ 's tubulation capacity by determining the ratio of the initial scattering intensity before addition of protein to the near-final scattering intensity ( $t = 2400$  to  $2500$  s) for each absorbance trace. Figure 1B shows the dramatic loss of  $\alpha\text{-Syn}_{100}$ -induced tubulation in the 1:1 PG:PC mixture compared with the 100% POPG vesicles. While  $\alpha\text{-Syn}_{100}$  causes a rapid decrease in the amount of light scattered by 100% POPG vesicles (Figure 1B inset), the signal change for the 1:1 PG:PC

vesicles is equivalent to that of the control.<sup>18</sup> Thus, we have confirmed that previous reports of reduced tubulation in 1:1 mixtures hold under conditions of equally bound protein.<sup>8,9</sup> As we will explore in depth below, this does not necessarily mean that the difference in binding energy does not dominate the biophysics of tubulation.

In order to begin to understand the remodeling phenomena that take place in 100% POPG yet are deficient in the 1:1 mixture, we turned to CGMD simulations. Time-averaged height surfaces,  $\langle h(x, y) \rangle$ , reflect the spontaneous curvature of a system by removing long-wavelength temporal fluctuations of the membrane.<sup>10</sup>  $\langle h(x, y) \rangle$  was determined using the method of our previous  $\alpha\text{-Syn}$  study (see the SI).<sup>10,52</sup> Figure 2A presents  $\langle h(x, y) \rangle$  for  $\alpha\text{-Syn}_{100}$  bound to pure POPG and 1:1 PG:PC bilayers determined over the last  $5 \mu\text{s}$  of the simulations.  $\alpha\text{-Syn}_{100}$  induces positive spontaneous curvature in both bilayers. We quantified  $\langle h(x, y) \rangle$  by determining the percent excess area for each system as  $(1 - A_{h(x,y)} / A_{xy}) \times 100\%$ , where  $A_{h(x,y)}$  is the area along the height surface and  $A_{xy}$  is the projected area (see the SI).<sup>53</sup> There is a significant increase in the percent excess area (Figure 2B, blue) in the POPG system (0.51%) compared with the 1:1 mixture (0.30%) (see Supplemental Table 1). On a per-protein basis, the magnitude of the induced spontaneous curvature appears to be small on the scale of global membrane remodeling. However, the cumulative effect imparted by multiple proteins organizing in a localized membrane region could induce enough curvature stress to breach the energy threshold required for membrane remodeling. As will be discussed below, recent work by the Voth group shed light on an important phenomenon where linear aggregation of N-BAR domain proteins occurs prior to macroscopic membrane remodeling.<sup>37</sup> A similar mechanism for protein aggregation/alignment may occur for  $\alpha\text{-Syn}_{100}$ , acting as local nucleation points for tubule formation. An additional set of simulations presented below will expand on this point.

It has been proposed that subtle changes in the depth of partitioning of an AH into the hydrophobic acyl-chain region can dramatically alter the induced (local) curvature and that this curvature is dependent on the membrane's hydrophobic thickness.<sup>29</sup> Figure 2C shows that  $\alpha\text{-Syn}_{100}$  partitions slightly deeper in the PG:PC mixture when the depth is measured relative to the lipid component density ( $Z_{\text{pep}}$ ) (results for all of the other 1600:1  $\alpha\text{-Syn}_{100}$  systems are presented in Supplemental Figure 2). However,  $Z_{\text{pep}}$  is not the most relevant measure of partition depth in the context of curvature induction.<sup>29</sup> We define the hydrophobic thickness of the membrane,  $2D_C$ , as the  $z$  distance between the points with equal probability for acyl-chain or solvent densities. There are two structural parameters that dictate the magnitude and sign of the induced spontaneous curvature: (1) the monolayer hydrophobic thickness  $D_C$  and (2) the extent to which the protein partitions into  $D_C$ .<sup>29</sup> Interestingly, for a given protein density (1600:1 or 400:1), regardless of the PC mole percent, the protein partitions to the same depth relative to  $D_C$  (see Supplemental Table 1). However, what does change with PC mole percent is the hydrophobic thickness (both in pure and protein systems), which increases by  $0.16 \text{ nm}$  in POPG relative to the 1:1 PG:PC mixture (see Supplemental Table 1). Although this shift is quite small—below the resolution of the MARTINI CG beads—current theory on AH curvature suggests that with equal relative partition depth, changes in hydrophobic thickness of  $0.2 \text{ nm}$  are capable of doubling the spontaneous curvature.<sup>29</sup> Thus, these data suggest a strong

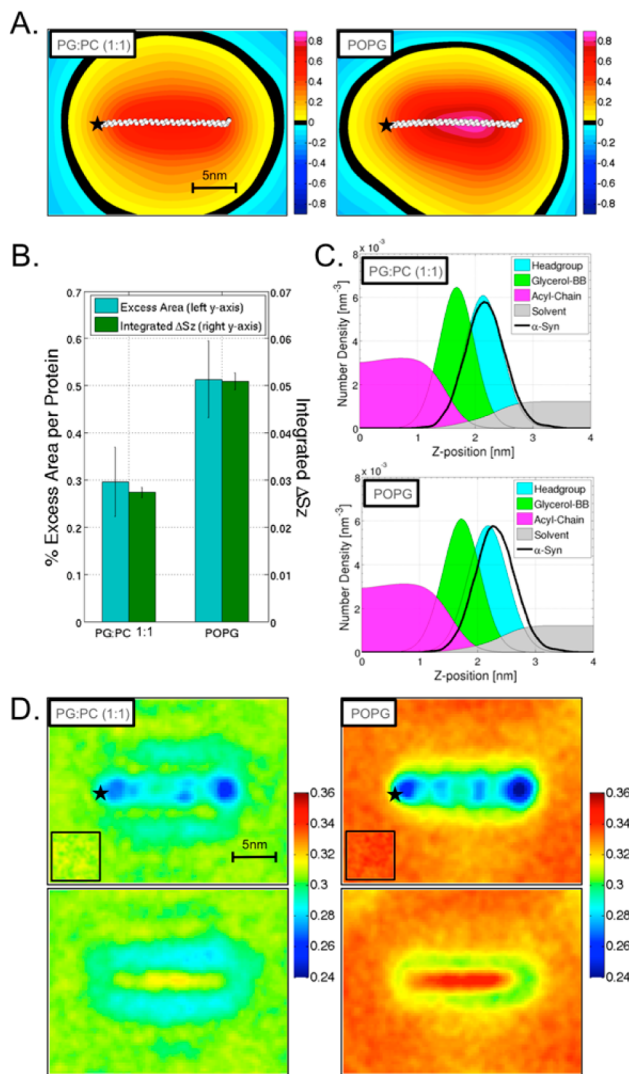


**Figure 2.** (A) Time-averaged height surfaces,  $\langle h(x, y) \rangle$ , for 1:1 PG:PC (left) and POPG (right), determined over the last 5  $\mu$ s of the simulations. Color map units are nm. (B) Percent excess area per protein (blue) and integrated total lipid order (green) for 1:1 PG:PC and POPG. (C) Lipid-component number density profiles for 1:1 PG:PC (top) and POPG (bottom) (solvent, gray; headgroup, cyan; carbonyl-glycerol, green; acyl-chain, magenta;  $\alpha$ -Syn<sub>100</sub>, black line). (D) Local total order parameter  $S_z(\bar{x}, \bar{y})$  for the membrane near the protein (top) and opposite the protein (bottom) in 1:1 PG:PC (left) and POPG (right) (warm colors = more ordered, cool colors = more disordered). The insets correspond to pure lipid  $S_z(\bar{x}, \bar{y})$  for each lipid composition. The location of the N-terminus of  $\alpha$ -Syn<sub>100</sub> is indicated with ★ (the protein itself is not shown).

correlation between hydrophobic thickness and curvature induction.

A shift in the membrane's hydrophobic thickness modulates how other structural features of the membrane respond to  $\alpha$ -Syn<sub>100</sub>'s relative partition depth, particularly the acyl-chain order parameter. We characterized the acyl-chain conformations around  $\alpha$ -Syn<sub>100</sub> using a local total lipid order parameter,  $S_z(\bar{x}, \bar{y})$  (see the SI for details of the method). Figure 2D illustrates  $S_z(\bar{x}, \bar{y})$  for the region of the monolayer near the protein (top) and opposite the protein (bottom) for the systems with 1:1 PG:PC (left) and POPG (right), with the corresponding data for protein-free bilayers given in the insets (see Supplemental Figures 2 and 3 for complete results for

other 1600:1  $\alpha$ -Syn<sub>100</sub> systems). The lipids near the protein are equally disordered for both systems, but the change relative to the bulk is much greater for POPG.

When we quantified  $S_z(\bar{x}, \bar{y})$  as a function of distance from the protein, we observed an asymmetry across the bilayer,  $\Delta S_z = S_{z,opposite} - S_{z,protein}$ . This asymmetry extends out to distances of 5 nm (Supplemental Figure 3E,F), with the largest asymmetry developing in the POPG system. When only the first shell of lipids is considered (by integration out to 1 nm from the protein), the order asymmetry shows a strong correlation with the excess area, where the POPG system again experiences twice the effect relative to the 1:1 mixture (Figure 2B, green bars). We speculate that because of the increased  $D_C$  in POPG, there is a greater volume beneath the protein that must be accommodated by the neighboring lipid's acyl chains, leading to more disordering of the lipids and giving rise to increased order asymmetry.

**Exploring the Role of Binding Affinity.** The simulation data comparing  $\alpha$ -Syn<sub>100</sub> in 100% PG and the 1:1 PG:PC mixture suggest, but in no way prove, a direct correlation between the depth of partition relative to the hydrophobic thickness, the order parameter asymmetry across the leaflets, the induced positive curvature, and tubulation. However, this correlation does not take into account the difference between the binding affinities for 100% POPG and the 1:1 PG:PC mixture. One explanation for the role of the affinity difference relates to the electrostatic repulsion between PG headgroups, which is lessened in the mixture. As a result, the 100% POPG membrane is under greater lateral pressure than that of the mixture. Binding of  $\alpha$ -Syn can relieve this pressure by screening lipid–lipid interactions through Lys–PG salt bridges. Although current theory<sup>29</sup> focuses on the importance of protein partition depth relative to hydrophobic thickness, it is possible that the protein inserts at the optimal  $Z_{pep}$  position (Figure 2C) for tubulation in the 100% PG bilayer.

Parsing the relative contributions of these driving forces—binding energy, partition depth, hydrophobic thickness, and order perturbations—is far from trivial. In an effort to isolate the binding-energy component, we engineered a minimally altered variant of  $\alpha$ -Syn<sub>100</sub> that would partition to the same depth in pure POPG bilayers (maintaining a constant  $D_C$  and local curvature induction) but have a reduced  $K_D$ .  $\alpha$ -Syn's membrane binding domain comprises seven imperfect heptad repeats with consensus sequence XKTKEGVXXXX (X = any residue).<sup>54</sup> We replaced the hydrophobic NAC domain (the sixth heptad) with a replicate of the fifth heptad (GAVV-TGVTAVA → EKTKEQVTNVG). The anticipated effect on  $K_D$  and the depth was uncertain, as the alteration reduces the hydrophobicity while adding extra charged residues (zero change in net charge). Because Lys residues in  $\alpha$ -Syn associate strongly with PG headgroups, we suggest that any reduction in measured binding affinity should be attributed to the loss in hydrophobicity.

We first tested the depth of partition and the order parameter asymmetry of this NAC-null protein using simulations, and Figure 3A shows that indeed the engineered variant has nearly identical binding depth and order parameter asymmetry as  $\alpha$ -Syn<sub>100</sub>. The NAC-null variant actually partitions slightly less deeply, and this is manifested in a slightly greater curvature field (Supplemental Table 1 and Supplemental Figure 4A–C). Experimentally, we found that the binding affinity of NAC-null was reduced 6-fold, which is considerably less of an effect than the lipid headgroup charge

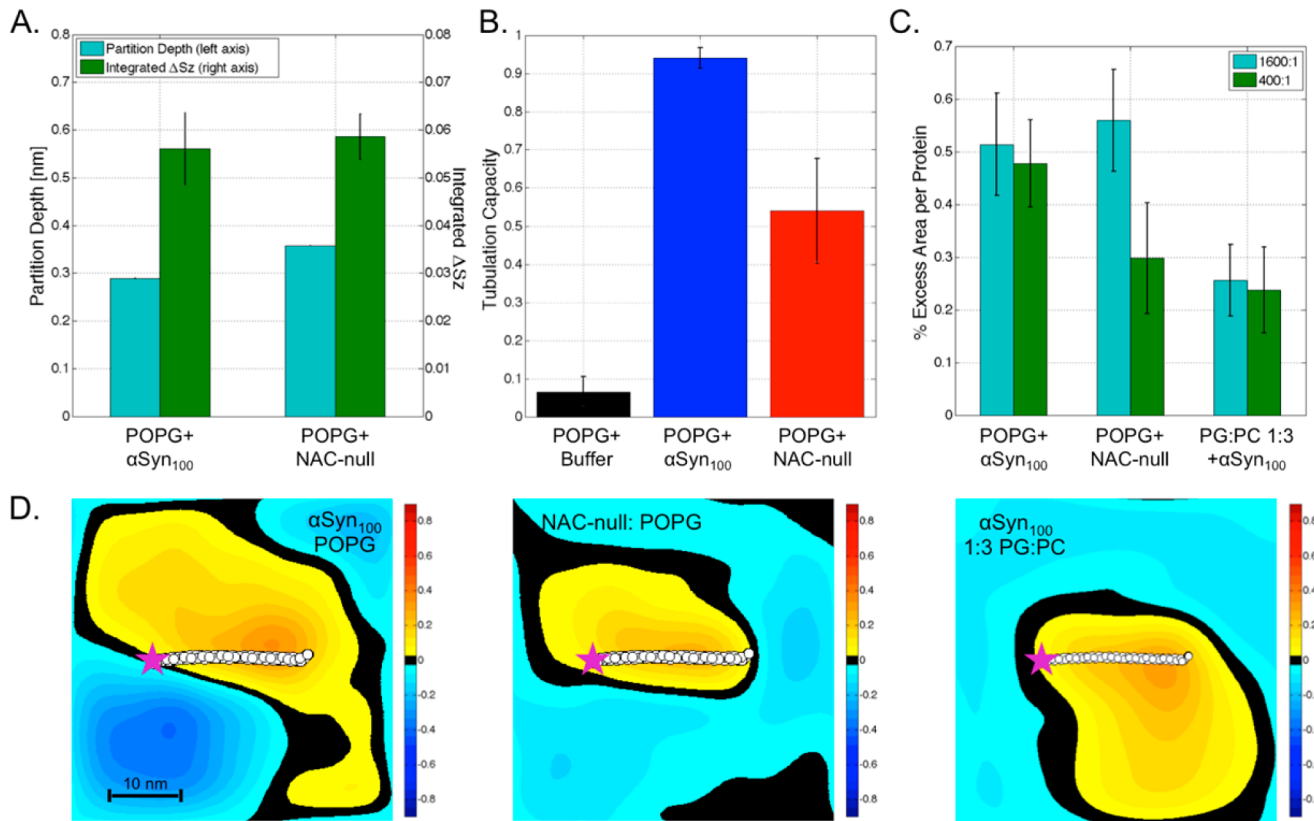


**Figure 3.** (A) Comparison of protein partition depths and integrated order parameter asymmetries for  $\alpha$ -Syn<sub>100</sub> (left) and NAC-null (right) proteins. (B) Experimental tubulation capacities at equal bound protein density for POPG + buffer (black), POPG +  $\alpha$ -Syn<sub>100</sub> (blue), and POPG + NAC-null (red). (C) Comparison of excess areas per protein for the low-density (1600:1, blue) and high-density (400:1, green) systems for  $\alpha$ -Syn<sub>100</sub> (left) and NAC-null (middle) in POPG and  $\alpha$ -Syn<sub>100</sub> in 1:3 PG:PC (right). (D) Time-averaged height surfaces for high-density (400:1)  $\alpha$ -Syn<sub>100</sub> (left) and NAC-null (middle) systems in POPG and  $\alpha$ -Syn<sub>100</sub> in 1:3 PG:PC (right). The average protein position is indicated with white spheres, and the N-terminus of the protein is indicated with ★.

with the native  $\alpha$ -Syn<sub>100</sub> sequence but significant nonetheless. We also found that at equal bound protein density, the NAC-null variant induced an approximately 50% reduction in tubulation (Figure 3B and Supplemental Figure 4D), also a smaller but significant effect. Thus, on the basis of the similar partition depths and order asymmetry along with the reduced  $K_D$ , the results for the engineered NAC-null construct strongly suggest that while there may be a range of partition depths over which tubulation is possible, the binding energy is a major player in dictating whether tubulation occurs.

Because the NAC-null variant shows decreased affinity relative to  $\alpha$ -Syn<sub>100</sub> in POPG despite the presence of extra Lys residues, it is likely that binding of the native protein (and possibly the stability of the bound protein–lipid complex) is in part driven by the hydrophobicity of the protein. Furthermore, given the ~60-fold reduction in affinity of  $\alpha$ -Syn<sub>100</sub> for 1:1 PG:PC versus POPG, an effect that has previously been shown to be electrostatically driven<sup>14,50,55</sup> these findings strongly suggest at least a two-stage binding process: (1) electrostatically driven adsorption of the unfolded protein and (2) a combination of electrostatic and hydrophobic stabilization of the  $\alpha$ -helical bound state.<sup>56</sup> We note that whereas our experiments capture the full-binding process, the simulations probe only the second stage. The implications of this two-stage binding will be discussed further.

Binding energy not only dictates the equilibrium distribution of bound and unbound protein but also reflects the strength (stability) of the interaction between the protein and the lipids

in its solvation shell. A tighter coupling—be it between charged (Lys/PG) or hydrophobic groups—should be manifested as a larger, more stable complex whose diffusion in the membrane will be slowed by size. This may increase the likelihood of stable, nucleating assemblies of proteins. In an attempt to more deeply understand the binding energy difference that dictates the reduced tubulation in the NAC-null variant, we simulated the two proteins ( $\alpha$ -Syn<sub>100</sub> and NAC-null) at high density on pure PG bilayers (for details, see Materials and Methods in the SI).

Figure 3D shows the calculated curvature fields for  $\alpha$ -Syn<sub>100</sub> (left) and NAC-null (middle). The  $\alpha$ -Syn<sub>100</sub> system shows a broad area of positive spontaneous curvature spanning well beyond the local region of a single protein (it should be noted that these images show a larger region of membrane than those in Figure 2A). The position and size of this curvature profile suggests stable protein–protein alignment that reinforces the curvature fields between proteins. Even though NAC-null induces a similar low-density curvature field and has the same depth and same order parameter asymmetry (Supplemental Figure 4), at high density it does not display the same curvature-field reinforcement as  $\alpha$ -Syn<sub>100</sub> (Figure 3D, middle). Quantification of these surfaces shows a 50% decrease in curvature capacity for high-density NAC-null (Figure 3C), matching the experimentally observed decrease in tubulation (Figure 3B) remarkably well.

Figure 3C shows that in the case of the native  $\alpha$ -Syn<sub>100</sub> sequence, the high-density per-protein curvature field recovers

that of the low-density (single-protein) case. This recovery is absent in the case of NAC-null, suggesting a loss of time-averaged helical alignment compared with the native sequence. We quantified this effect by time-averaged distance matrices for amino acids in nearest-neighbor protein–protein pairs (Supplemental Figure 5). By observing the temporal stability within these distance matrices (or lack thereof), we asked the following question: Does the stability of specific protein–protein alignment motifs (which may correlate with binding energy) correlate with stabilization of long-range curvature fields? Despite limited sampling, the data are consistent with the notion that the reinforcement of the curvature fields in  $\alpha$ -Syn<sub>100</sub> correlates with stabilization of protein–protein alignments. As hypothesized, in the case of  $\alpha$ -Syn<sub>100</sub> the proteins sample a relatively tight window of possible alignment states (25.2% unique states sampled). Most interestingly, the NAC-null results show a marked increase in the transitions between states (50.4%).

#### Depth of Partition/Hydrophobic Thickness or Binding Affinity?

The most recent theory for AH-induced curvature induction suggests a small range of depths over which positive curvature will be induced for a given hydrophobic thickness. As proteins partition more deeply into the bilayer, the effect is lost and can even be reversed to produce negative curvature.<sup>29</sup> The data presented thus far do not directly address this because relative to  $D_C$  the simulated proteins all partitioned to the same depth. In a purely computational experiment, we manipulated this partitioning by artificially varying the charge of  $\alpha$ -Syn<sub>100</sub> (via computational point mutations) within the same lipid mixture (i.e., the same  $D_C$ ). Indeed, the results confirmed a high sensitivity of the curvature to subtle changes in depth. For example, we showed the ability to turn a 100% PC bilayer with  $\alpha$ -Syn<sub>100</sub> (deep partitioning, small  $D_C$ , low curvature) into a PG-like bilayer (shallow partitioning, small  $D_C$ , high curvature). While  $\alpha$ -Syn<sub>100</sub> does not bind pure PC bilayers in the fluid phase, this computational exercise is valuable in the context of understanding the driving forces for curvature induction. These data are presented in Supplemental Figure 6.

In this context, interpretation of the lost tubulation in the PG:PC mixture, where the protein depth relative to  $D_C$  is invariant, is complicated by the concomitant decreases in curvature and affinity. In order to exaggerate the relationship among depth, hydrophobicity, and curvature, we simulated a 400:1 system in a 1:3 PG:PC mixture. In this mixture, the protein again partitions to the same position relative to  $D_C$  as in POPG. Surprisingly, when we calculated the distance matrix for interacting proteins in PG:PC mixtures, we found similar (or even reduced) mobility as in the wild type (Supplemental Figure 5D). Similar to the 400:1 POPG system, this reduced mobility is accompanied by a reinforcement of local curvature fields (Figure 3C,D), although the stabilized curvature field is less than half as intense. We can explain the reduced curvature intensity as a result of a 0.14 nm reduction in  $D_C$  in going from the 400:1 POPG system to the 1:3 PG:PC system. This explanation is appealing in light of the lost tubulation. However, in view of the dramatically reduced binding affinity that we measured experimentally, along with the observation of increased mobility of NAC-null, the reduced mobility of the protein was perplexing. However, in the context of a two-stage binding process and the fact that our experiments were performed at equal bound protein density, interpretation of the data becomes possible. The loss in binding affinity likely reflects a loss in electrostatic attraction between the unfolded, soluble

protein and the lipid headgroups. However, once adsorbed, the folded and bound protein is stabilized by a solvating lipid shell, primarily through Lys–PG contacts. In 100% PG, the lipids are free to bind and unbind the protein without great penalty, as the Lys groups can be immediately stabilized by another PG. On the other hand, in the PG:PC mixture, lipid exchange is likely slowed by the penalty of replacing a Lys–PG contact with a Lys–PC contact. Thus, lipid diffusion (binding/unbinding) could be expected to be slowed in the PG:PC mixture. On average this may slow protein diffusion because the time-averaged lipid–protein complex will be more stable. Our simulations are not sampled well enough to test this long-time-scale phenomenon with statistical certainty.

Figure 4 summarizes much of the relevant data presented thus far. As stated above, there is a systematic increase in

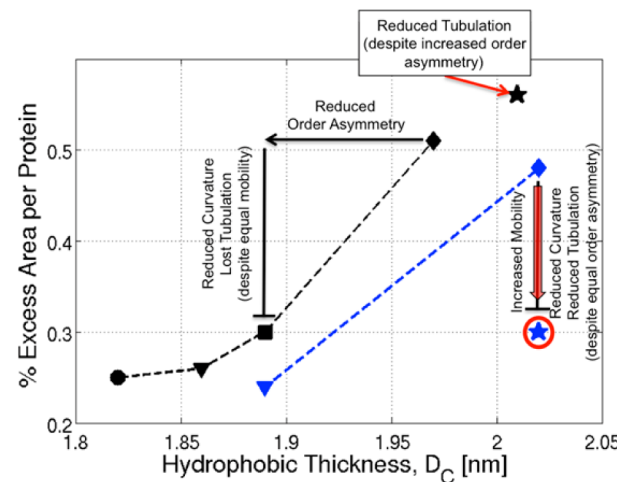


**Figure 4.** Excess area as a function of hydrophobic thickness. Colors demarcate low-density (1600:1, black) vs high-density (400:1, blue). Symbols indicate lipid composition: ● = POPC; ▼ = 1:3 PG:PC; ■ = 1:1 PG:PC; ♦ = POPG. The ★ denotes NAC-null. Annotations are as described in the text.

hydrophobic thickness of native  $\alpha$ -Syn<sub>100</sub>-containing bilayers as the PG density increases (Figure 4, black dashed line). As the hydrophobic thickness decreases from ~2.0 to ~1.9 nm, there is reduced lipid order asymmetry that correlates with a reduction in curvature and is consistent with loss of tubulation capacity. When we incorporate the data for the NAC-null systems, in particular the result at high density, this correlation fails. The NAC-null protein partitions less shallow than  $\alpha$ -Syn<sub>100</sub>, inducing an even greater hydrophobic thickness and lipid order asymmetry (curvature) (Figure 4, black ★); experimentally, however, NAC-null has a reduced tubulation capacity. For these reasons, we conclude that lipid order asymmetry (lost in the native sequence at 1:3 PG:PC) is necessary but not sufficient (present in NAC-null) for tubulation.

Figure 4 also reiterates the point that at high density (400:1), PG:NAC-null and 1:3 PG:PC +  $\alpha$ -Syn<sub>100</sub> induce approximately the same amount of per-protein curvature. This shows that these induced curvature fields alone do not directly correlate with tubulation, as the NAC-null variant does tubulate vesicles (albeit 50% less than pure PG). How can we reconcile this apparent disparity in induced curvature and tubulation capacity? The data suggest that even if a protein partitions to the appropriate depth in a membrane with sufficient hydro-

phobic thickness (and therefore imparts sufficient lipid order asymmetry), the tubulation capacity is reduced if stable protein–lipid complex interactions are not established (as in NAC-null). However, in the 400:1 1:3 PG:PC +  $\alpha$ -Syn<sub>100</sub> system, stable protein–lipid complex interactions are formed, as evidenced by the stabilized curvature field (Figure 3D) and the reduced protein mobility (Supplemental Figure 5D), yet reduced lipid order asymmetry reduces the stress on the membrane below the tubulation threshold. Therefore, we conclude that stability of the protein in the bound state (lost in NAC-null) is a necessary but not sufficient (present in the native sequence at 1:3 PG:PC) component of the tubulation mechanism.

Thus, it appears that two constraints must be met in order for  $\alpha$ -Syn<sub>100</sub> to tubulate a vesicle: (1) it must bind with sufficient energy to slow the protein/lipid dynamics and allow for nucleation of pretubule assemblies<sup>37</sup> and (2) it must bind in a narrow window of depths, inducing a particular hydrophobic thickness that can promote sufficient per-protein curvature. Furthermore, because the NAC-null variant still maintains some tubulation activity, there must be a driving force present in the NAC-null and POPG  $\alpha$ -Syn<sub>100</sub> systems but not in 1:3 PG:PC, one that is not dependent on strong binding affinity and drives the formation of a tubule. We propose that this driving force is the energetic penalty of induced lipid order asymmetry across the leaflets.

**Relief of Order Parameter Asymmetry as an Additional Driving Force for Tubulation.** For  $\alpha$ -Syn<sub>100</sub> to induce tubulation of a large vesicle, the local effects of a single  $\alpha$ -Syn<sub>100</sub> must propagate to neighboring proteins.<sup>37,57</sup> We speculate that there exists a reinforced/nucleating  $\alpha$ -Syn<sub>100</sub> structure with high order asymmetry and that resolution of this asymmetry may drive tubulation. No experimental information is available to suggest that such structures exist or to provide hints concerning what those structures might look like. In a modest effort to gain insight into how large-scale assemblies may promote tubulation, we ran three simulations with hand-built assemblies (consisting of 48 proteins) embedded in a POPG membrane. We recognize that these tubule simulations sample only three possible nucleating structures and acknowledge that other computational techniques (including more aggressive coarse graining<sup>58</sup> and mesoscopic modeling<sup>59,60</sup>) may be better-suited for such investigations. Nonetheless, this approach has allowed us to investigate the possible behaviors of acyl chains in the remodeling process. Each system contained 85 296 lipids (5 200 608 total CG beads) and 48 proteins arranged in one of three unique conformations (spoke, circumferential, and carpet). The local protein density for each system (defined as the protein:lipid ratio within 1 nm of the protein) was set at ~1:50, just below the experimental saturation density observed with anionic and zwitterionic/anionic lipid mixtures.

Figure 5 displays the initial starting configuration and the final snapshot for the spoke conformation. The circumferential and carpet conformations are presented in Supplemental Figure 7. For all three protein conformations, membrane remodeling occurred very rapidly. During the first ~40 ns, an initial invagination spanned the central ring of the membrane encompassing the inner 5 nm of the protein spokes. By 100 ns, the initial depression inverted and the budding tubule began to take shape. By ~300 ns there was a fully formed nascent tubule (~25 nm in height) surrounded by undulating POPG bilayer. This structure changed only slightly between 300 and 850 ns. It is possible that if these simulations were allowed to

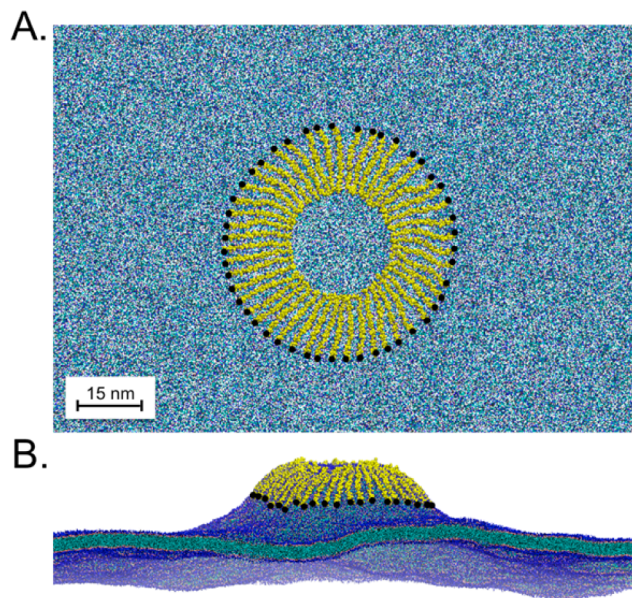
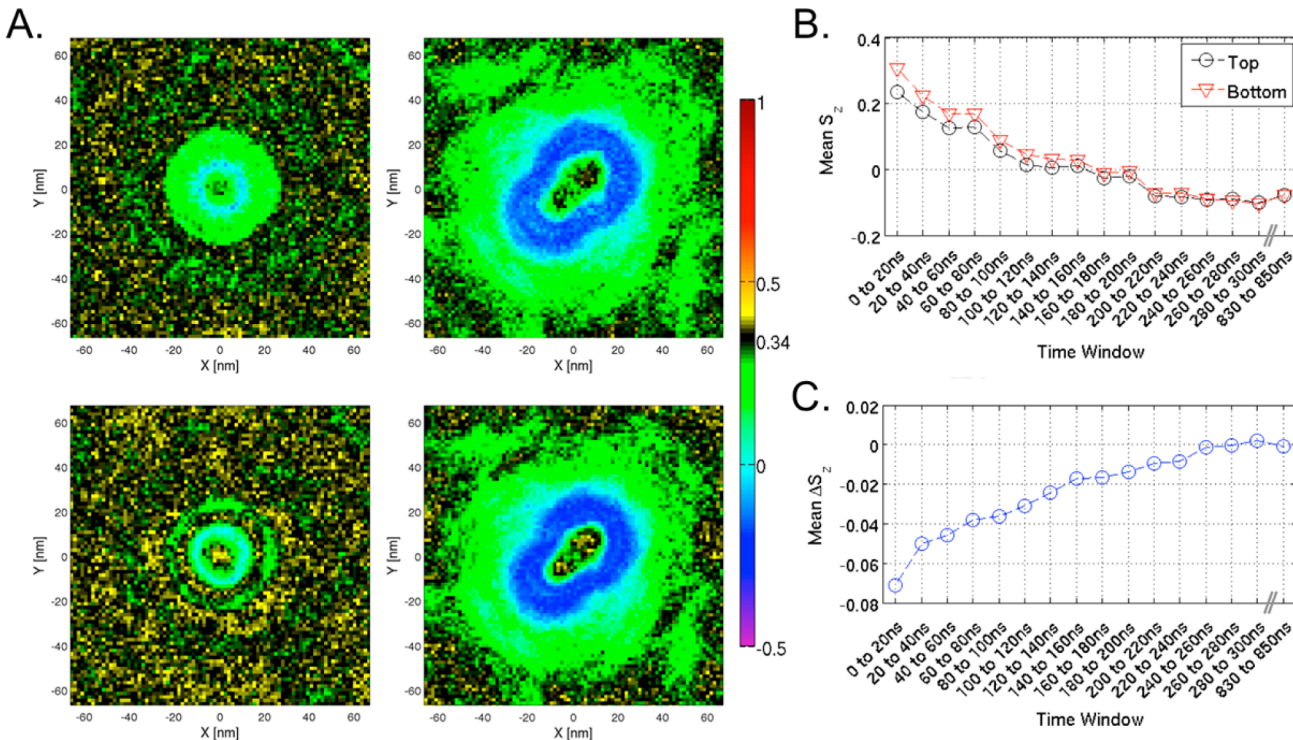


**Figure 5.** (A) Top-down view of the spoke starting configuration. The system includes 48  $\alpha$ -Syn<sub>100</sub> proteins (yellow) and 85 296 POPG lipids (blue). Waters have been removed for clarity. The N-terminus of each protein is indicated by ●. (B) Snapshot at 300 ns simulation time. The budding tubule extends ~25 nm above the bulk lipid bilayer.

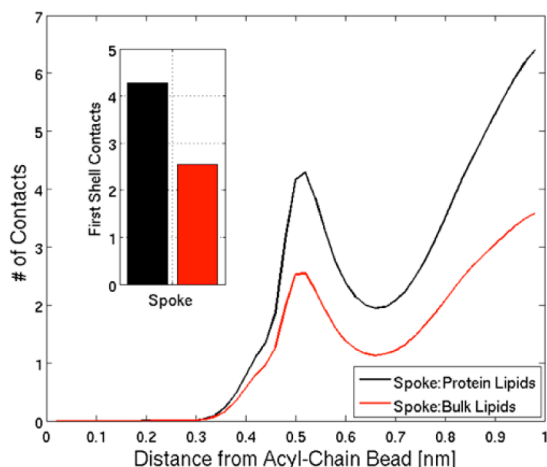
run for much longer times, the highly ordered protein conformation might diffuse apart. While we cannot rule this out, we do note that after 300 ns the carpet conformation began to realign into radial (spoke) and circumferential orientations to orient  $\alpha$ -Syn to the tubule's curvature field (Supplemental Figure 9D).

Figure 6A shows the total lipid order parameter  $S_z(\bar{x}, \bar{y})$  for the protein monolayer (top) and the opposite monolayer (bottom) calculated over the first 20 ns (left) and the last 20 ns (right) of the simulation of the spoke conformation (results for the circumferential and carpet conformations are presented in Supplemental Figures 8 and 9, respectively). In all three systems, there is a large shift in the total lipid order toward greater disorder and eventually the formation of antialigned chains [i.e., negative  $S_z(\bar{x}, \bar{y})$ ]. As the tubule forms, this shift in order is accompanied by a transition toward a symmetric  $S_z(\bar{x}, \bar{y})$  profile across the bilayer (Figure 6B,C and Supplemental Figures 8 and 9). By the end of the tubulation event, the two monolayers have similar  $S_z(\bar{x}, \bar{y})$  profiles [see Supplemental Figure 10 for the detailed time course of  $S_z(\bar{x}, \bar{y})$  for the spoke conformation]. This change is different than the changes observed for the low-density  $\alpha$ -Syn<sub>100</sub> systems (Figure 2D and Supplemental Figure 3) where a stable asymmetry is established. Because of the high protein density, the limited numbers of lipids near the protein are forced to accommodate the void volume beneath each protein, inducing increased splay away from the local normal.

At the core of the protein assembly, the increased splay is significant enough to drive antialignment of the acyl chains (chain orientation orthogonal to the local bilayer normal). This antialignment propagates across the bilayer, suggesting that a monolayer coupling occurs. We quantified this monolayer coupling by determining the total number of interleaflet acyl-chain contacts in regions near the protein and regions in the bulk membrane. Figure 7 shows the distance distributions of contacts for the spoke conformation. The number of first-shell



**Figure 6.** (A)  $S_z(\bar{x}, \bar{y})$  for the protein-containing leaflet (top) and opposite leaflet (bottom) at the early stage (0 to 20 ns, left) and the late tubule stage (830 to 850 ns, right). The color map reference (black) is set at  $S_z$  for pure POPG. (B) Time course of the mean  $S_z$  for the protein (black) and opposite (red) monolayers as the tube develops. (C) Time course of the average difference  $\Delta S_z$  across the membrane ( $\Delta S_z = S_{z,\text{opposite}} - S_{z,\text{protein}}$ ).



**Figure 7.** Total number of interleaflet contacts (acyl-chain-to-acyl-chain) for lipids near the protein (black) vs lipids in the bulk (red) in the spoke conformation. The number of first-shell contacts is quantified in the inset.

acyl-chain-to-acyl-chain interactions (inset) exhibits an ~2-fold increase in the number of contacts near the protein relative to the bulk. This is a consistent trend for all three protein conformations (see Supplemental Figure 11).

## DISCUSSION

Numerous computational studies have explored protein-driven membrane remodeling.<sup>10,15,19,22,26,37–41,43,57,61</sup> A major focus of many of these studies has been on BAR-domain proteins. BAR-domain proteins are a curvature-inducing class of proteins that can contain both a rigid scaffolding and an AH domain, and similar to  $\alpha$ -Syn,<sup>8,11</sup> these proteins have been shown to both

sense and generate curvature.<sup>16–18,25,36,42,62</sup> In N-BAR proteins, the AH plays an essential role in curvature generation and the stability of the membrane tube by stabilizing dimer–dimer interactions and propagating the N-BAR lattice along the membrane.<sup>19,39</sup> Furthermore, evidence exists that the AH, and not the scaffolding domain, is responsible for the protein's curvature-sensing abilities.<sup>16,17,24</sup> AH curvature induction can be so extreme as to promote membrane scission, as is the case for the ENTH domain of epsin<sup>21</sup> and the monomeric family of synucleins ( $\alpha$ -Syn,  $\beta$ -Syn, and  $\gamma$ -Syn<sup>6,8,11</sup>). There is a balance between the remodeling effects induced by the rigid scaffold and those driven by the AH, and elucidating the role of each mechanism remains an active area of investigation.<sup>62</sup>

There are several potential complementary mechanisms for  $\alpha$ -Syn-induced membrane curvature and tubulation. We have shown that at equal bound density the protein has a dramatically reduced effect on tubulation of PG:PC mixtures compared with POPG bilayers. We correlated this effect with an experimentally measured decrease in binding affinity (~60-fold) and a simulated increase in hydrophobic thickness, partition depth, and order parameter asymmetry. This finding raised the question of whether depth and order asymmetry alone can explain tubulation differences. To at least in part address this, we designed an  $\alpha$ -Syn variant lacking the NAC domain (NAC-null), which we predicted would have reduced affinity but partition to approximately the same depth as wild-type  $\alpha$ -Syn in POPG vesicles having consistent hydrophobic thickness. Removal of the NAC did in fact reduce binding to POPG vesicles (by ~1 order of magnitude). This more mild reduction in affinity correlates with a more mild reduction in tubulation, despite the fact that the NAC-null mutant partitions to a slightly less shallow depth than the wild-type protein (and actually slightly increases the induced curvature field) and has

the same impact on the order parameter asymmetry. This finding suggests that depth and order asymmetry alone do not explain the reduction in tubulation, though it certainly does not rule out their potential contribution in the case of the PG:PC mixture (Supplemental Figure 5D). Rather, our simulations suggest that the NAC domain may be essential in stabilizing protein–lipid complexes and, in so doing, promoting organization on the bilayer surface. Indeed, a very recent study supports our findings on the importance of the hydrophobic core of the NAC domain in  $\alpha$ -Syn-induced membrane remodeling. Using supported lipid bilayers, that study shows a loss of induced membrane defects and reduced membrane-bound protein cluster size with an  $\alpha$ -Syn variant lacking the hydrophobic sixth heptad.<sup>63</sup>

In a recent study, Lipowsky discussed how the adhesion energy of an adsorbing particle can induce spontaneous membrane curvature.<sup>20</sup> Using N-BAR as an example, the theory predicted that the remodeling capacity of the N-BAR scaffolding domain is directly coupled to the adhesion energy it gains upon interacting with the membrane. If the adsorbing N-BAR protein imparts sufficient adhesion energy with the membrane (i.e., greater than the bending energy required to deform the bilayer), the membrane will buckle and adopt the intrinsic curvature of the protein. Recent work from the Voth group has characterized the role of binding energy for exactly this N-BAR/membrane system<sup>37</sup>. Using their recently developed hybrid CG model, the authors varied the CG N-BAR binding affinity for the lipid headgroup. In doing so, they were able both to inhibit protein aggregation and macroscopic membrane remodeling (low adhesion energy) and to induce disruptions and tears within the membrane (high adhesion energy). Because  $\alpha$ -Syn lacks a scaffolding domain, the notion of adhesion energy must be taken in a slightly different context. Instead of the adhesion energy coupling the membrane to a rigid scaffold domain, weaker binding would increase lipid exchange within the lipid solvent shell around the protein. Speculatively, this would have the effect of destabilizing the protein–lipid complex, potentially accelerating the protein dynamics on the surface and reducing the likelihood of nucleating stable protein assemblies.

This is not to say that partition depth and hydrophobic thickness are not significant. It was surprising to us that given similar relative partition depths, such a small change in the hydrophobic thickness in the PG:PC mixture ( $\sim 0.16$  nm thinner than PG) might correspond to a such a large experimental observable. However, the recent theory of AH curvature induction developed by May's group predicts a partition depth and hydrophobic thickness dependence on the spontaneous curvature and bending rigidity of a membrane.<sup>29</sup> As the hydrophobic thickness increases, the range and magnitude of the predicted spontaneous curvature is expanded (e.g., an increase of 0.2 nm in  $2D_C$ —on the order of the difference we observed between pure PG and the 1:1 mixture—corresponds to a doubling of the curvature intensity for the same partition depth).<sup>29</sup> All of this leads to the following question: Are individual curvature fields the necessary piece, or is it organization of the fields that dominates? Perhaps it is a combination of the two. Our simulation and experimental results suggest that lipid order asymmetry (either through protein partition depth or membrane hydrophobicity) and binding affinity are both necessary but not sufficient components of the AH tubulation mechanism.

More generally speaking, increased spontaneous curvature is the result of an area mismatch between monolayers, and it has been shown experimentally through the use of transiently asymmetric lipid vesicles (protein-free) that an increase in area mismatch by as little as  $\sim 1\%$  is enough to initiate the macroscopic remodeling of lipid vesicles.<sup>53,64</sup> In those experiments, the transient asymmetry relaxed with time as a result of lipid flip-flop. The rate of lipid flip-flop is typically very low (corresponding to a time scale of minutes to hours) in pure lipid vesicles. However, AHs have been shown to greatly enhance lipid flip-flop rates.<sup>65,66</sup> In the case of  $\alpha$ -Syn tubulation experiments, where a high concentration of  $\alpha$ -Syn is added to solution, the relationship among binding kinetics, protein reorganization (e.g., into organized pretubule structures), the development of local curvature stresses and the resulting curvature fields, lipid flip-flop, and tubulation remains unknown. In one scenario, where binding is presumed to be much faster than tubulation, every lipid in the outer leaflet of the vesicle would be occupied in forming the solvation shell of a neighboring protein. In that case, it seems unlikely that lipid flip-flop would be favorable.

Our simulations were designed to test a second scenario in which the nucleation of tubules occurs rapidly and locally. Indeed, high local densities can induce curvature and recruit more proteins.<sup>37</sup> In this case, accelerated local lipid flip-flop seems likely in order to relieve the local curvature strain. In order to test this, we eliminated the area mismatch between the leaflets: the small systems had protein on both leaflets, while in the large systems (protein in only one leaflet) we eliminated the excess area by removing lipids. This choice was made in order to probe whether the proteins themselves can still cause remodeling and tubulation in the case where there is time for lipid flip-flop. Indeed, we showed that they can do so.

Previous work by our group has focused on the coupling of lipid order across the bilayer leaflets, where we identified acyl-chain interdigitation as central to the propagation of order across monolayers in phase-separated bilayers.<sup>67</sup> In the case of the  $\alpha$ -Syn tubulation simulations presented here, we have also observed interleaflet coupling, though the character of the interdigitation is quite different. As a tubule develops, lipids in both monolayers adopt an antialigned conformation, increasing favorable chain–chain interactions between the monolayers (see Figure 6 and Supplemental Figure 11). The drive toward order parameter symmetry observed in the tubulation simulations, which is coupled to these additional contacts, may provide an important additional piece of the biophysical driving force for tubulation.

In this study we have discussed  $\alpha$ -Syn<sub>100</sub>-induced membrane remodeling/tubulation in the context of *in vitro* studies showing that  $\alpha$ -Syn tubulates synthetic vesicles.<sup>8,68</sup> *In vivo*,  $\alpha$ -Syn has been shown to interact with both the inner and outer membranes of the mitochondria.<sup>7,69</sup> Overexpressed  $\alpha$ -Syn, which is associated with Parkinson's disease,<sup>70–72</sup> induces fragmentation of mitochondria and impairs mitochondria complex 1 activity.<sup>7</sup> Mitochondria have  $\sim 15\%$  anionic lipids, the majority of which is cardiolipin (an anionic lipid with four acyl chains and a headgroup charge of  $-2$ ).<sup>73</sup> Indeed,  $\alpha$ -Syn has a high binding affinity for cardiolipin.<sup>73</sup> This association of  $\alpha$ -Syn with mitochondria coupled with its affinity for cardiolipin lead us to predict that many of the mechanisms discussed here are at play in this pathological condition. The different structural characteristics of cardiolipin may result in a unique

remodeling capacity relative to more typical anionic phospholipid mixtures (e.g., POPG:POPC).

## ■ ASSOCIATED CONTENT

### § Supporting Information

Detailed Materials and Methods section; lipid structure and schematic for system construction (Supplemental Figure 1); full detail of height surfaces and protein depth profiles for  $\alpha$ -Syn<sub>100</sub> (Supplemental Figure 2); full detail of total lipid order results (Supplemental Figure 3); NAC-null simulation results (Supplemental Figure 4); distance matrices for the 400:1 systems (Supplemental Figure 5);  $\alpha$ -Syn:mod1,2 results (Supplemental Figure 6); tubule simulation results for all three protein conformations (Supplemental Figures 7–10); interleaflet acyl-chain contacts (Supplemental Figure 11); and a summary of protein partition depths and membrane hydrophobic thicknesses (Supplemental Table 1). This material is available free of charge via the Internet at <http://pubs.acs.org>.

## ■ AUTHOR INFORMATION

### Corresponding Author

jnsachs@umn.edu

### Notes

The authors declare no competing financial interest.

## ■ ACKNOWLEDGMENTS

This work was supported in part by the National Institutes of Health (R01 NS084998-01 to J.N.S.; NRSA Fellowship F31 NS077634-02 to A.R.B.; GM102815 to E.R.; and Predoctoral Training Grant GM008283 to V.C.D. and M.M.L.). We also acknowledge D. C. DeWitt for assistance in cloning the NAC-null construct. All simulations and analyses were completed at the Minnesota Supercomputing Institute (MSI).

## ■ REFERENCES

- Robotta, M.; Braun, P.; van Rooijen, B.; Subramaniam, V.; Huber, M.; Drescher, M. *ChemPhysChem* **2011**, *12*, 267.
- Georgieva, E. R.; Ramlall, T. F.; Borbat, P. P.; Freed, J. H.; Eliezer, D. *J. Biol. Chem.* **2010**, *285*, 28261.
- Trexler, A. J.; Rhoades, E. *Biochemistry* **2009**, *48*, 2304.
- Georgieva, E. R.; Ramlall, T. F.; Borbat, P. P.; Freed, J. H.; Eliezer, D. *J. Am. Chem. Soc.* **2008**, *130*, 12856.
- Jao, C. C.; Hegde, B. G.; Chen, J.; Haworth, I. S.; Langen, R. *Proc. Natl. Acad. Sci. U.S.A.* **2008**, *105*, 19666.
- Kamp, F.; Exner, N.; Lutz, A. K.; Wender, N.; Hegermann, J.; Brunner, B.; Nuscher, B.; Bartels, T.; Giese, A.; Beyer, K.; Eimer, S.; Winklhofer, K. F.; Haass, C. *EMBO J.* **2010**, *29*, 3571.
- Nakamura, K.; Nemaní, V. M.; Azarbal, F.; Skibinski, G.; Levy, J. M.; Egami, K.; Munishkina, L.; Zhang, J.; Gardner, B.; Wakabayashi, J.; Sesaki, H.; Cheng, Y.; Finkbeiner, S.; Nussbaum, R. L.; Maslia, E.; Edwards, R. H. *J. Biol. Chem.* **2011**, *286*, 20710.
- Varkey, J.; Isas, J. M.; Mizuno, N.; Jensen, M. B.; Bhatia, V. K.; Jao, C. C.; Petrolva, J.; Voss, J. C.; Stamou, D. G.; Steven, A. C.; Langen, R. *J. Biol. Chem.* **2010**, *285*, 32486.
- Jiang, Z.; de Messieres, M.; Lee, J. C. *J. Am. Chem. Soc.* **2013**, *135*, 15970.
- Braun, A. R.; Sevcik, E.; Chin, P.; Rhoades, E.; Tristram-Nagle, S.; Sachs, J. N. *J. Am. Chem. Soc.* **2012**, *134*, 2613.
- Westphal, C. H.; Chandra, S. S. *J. Biol. Chem.* **2013**, *288*, 1829.
- Taneva, S. G.; Lee, J. M.; Cornell, R. B. *Biochim. Biophys. Acta* **2012**, *1818*, 1173.
- Jensen, M. B.; Bhatia, V. K.; Jao, C. C.; Rasmussen, J. E.; Pedersen, S. L.; Jensen, K. J.; Langen, R.; Stamou, D. *J. Biol. Chem.* **2011**, *286*, 42603.
- Middleton, E. R.; Rhoades, E. *Biophys. J.* **2010**, *99*, 2279.
- Perlmutter, J. D.; Braun, A. R.; Sachs, J. N. *J. Biol. Chem.* **2009**, *284*, 7177.
- Madsen, K. L.; Bhatia, V. K.; Gether, U.; Stamou, D. *FEBS Lett.* **2010**, *584*, 1848.
- Bhatia, V. K.; Madsen, K. L.; Bolinger, P. Y.; Kunding, A.; Hedegard, P.; Gether, U.; Stamou, D. *EMBO J.* **2009**, *28*, 3303.
- Zhu, C.; Das, S. L.; Baumgart, T. *Biophys. J.* **2012**, *102*, 1837.
- Cui, H.; Mim, C.; Vazquez, F. X.; Lyman, E.; Unger, V. M.; Voth, G. A. *Biophys. J.* **2013**, *104*, 404.
- Lipowsky, R. *Faraday Discuss.* **2013**, *161*, 305.
- Boucrot, E.; Pick, A.; Camdere, G.; Liska, N.; Evergren, E.; McMahon, H. T.; Kozlov, M. M. *Cell* **2012**, *149*, 124.
- Cui, H.; Lyman, E.; Voth, G. A. *Biophys. J.* **2011**, *100*, 1271.
- Drin, G.; Antonny, B. *FEBS Lett.* **2010**, *584*, 1840.
- Bhatia, V. K.; Hatzakis, N. S.; Stamou, D. *Semin. Cell Dev. Biol.* **2010**, *21*, 381.
- Hatzakis, N. S.; Bhatia, V. K.; Larsen, J.; Madsen, K. L.; Bolinger, P. Y.; Kunding, A. H.; Castillo, J.; Gether, U.; Hedegard, P.; Stamou, D. *Nat. Chem. Biol.* **2009**, *5*, 835.
- Arkhipov, A.; Yin, Y.; Schulten, K. *Biophys. J.* **2009**, *97*, 2727.
- Campelo, F.; McMahon, H. T.; Kozlov, M. M. *Biophys. J.* **2008**, *95*, 2325.
- Campelo, F.; Fabrikant, G.; McMahon, H. T.; Kozlov, M. M. *FEBS Lett.* **2010**, *584*, 1830.
- Zemel, A.; Ben-Shaul, A.; May, S. *J. Phys. Chem. B* **2008**, *112*, 6988.
- Fernandes, F.; Loura, L. M.; Chichon, F. J.; Carrascosa, J. L.; Fedorov, A.; Prieto, M. *Biophys. J.* **2008**, *94*, 3065.
- Drin, G.; Casella, J. F.; Gautier, R.; Boehmer, T.; Schwartz, T. U.; Antonny, B. *Nat. Struct. Mol. Biol.* **2007**, *14*, 138.
- Cornell, R. B.; Taneva, S. G. *Curr. Protein Pept. Sci.* **2006**, *7*, 539.
- Ulmer, T. S.; Bax, A.; Cole, N. B.; Nussbaum, R. L. *J. Biol. Chem.* **2005**, *280*, 9595.
- Chandra, S.; Chen, X.; Rizo, J.; Jahn, R.; Sudhof, T. C. *J. Biol. Chem.* **2003**, *278*, 15313.
- Crowet, J. M.; Lins, L.; Dupiereux, I.; Elmoualija, B.; Lorin, A.; Charlotteaux, B.; Stroobant, V.; Heinen, E.; Brasseur, R. *Proteins* **2007**, *68*, 936.
- Sorre, B.; Callan-Jones, A.; Manzi, J.; Goud, B.; Prost, J.; Bassereau, P.; Roux, A. *Proc. Natl. Acad. Sci. U.S.A.* **2012**, *109*, 173.
- Simunovic, M.; Srivastava, A.; Voth, G. A. *Proc. Natl. Acad. Sci. U.S.A.* **2013**, *110*, 20396.
- Simunovic, M.; Mim, C.; Marlovits, T. C.; Resch, G.; Unger, V. M.; Voth, G. A. *Biophys. J.* **2013**, *105*, 711.
- Mim, C.; Cui, H.; Gawronski-Salerno, J. A.; Frost, A.; Lyman, E.; Voth, G. A.; Unger, V. M. *Cell* **2012**, *149*, 137.
- Lyman, E.; Cui, H.; Voth, G. A. *Biophys. J.* **2010**, *99*, 1783.
- Yin, Y.; Arkhipov, A.; Schulten, K. *Structure* **2009**, *17*, 882.
- Arkhipov, A.; Yin, Y.; Schulten, K. *Biophys. J.* **2008**, *95*, 2806.
- Blood, P. D.; Voth, G. A. *Proc. Natl. Acad. Sci. U.S.A.* **2006**, *103*, 15068.
- Van der Spoel, D.; Lindahl, E.; Hess, B.; Groenhof, G.; Mark, A. E.; Berendsen, H. J. C. *J. Comput. Chem.* **2005**, *26*, 1701.
- Hess, B.; Kutzner, C.; van der Spoel, D.; Lindahl, E. *J. Chem. Theory Comput.* **2008**, *4*, 435.
- Marrink, S. J.; Risselada, H. J.; Yefimov, S.; Tieleman, D. P.; de Vries, A. H. *J. Phys. Chem. B* **2007**, *111*, 7812.
- de Jong, D. H.; Singh, G.; Bennett, W. F. D.; Arnarez, C.; Wassenaar, T. A.; Schäfer, L. V.; Periole, X.; Tieleman, D. P.; Marrink, S. J. *J. Chem. Theory Comput.* **2013**, *9*, 687.
- Brandt, E. G.; Braun, A. R.; Sachs, J. N.; Nagle, J. F.; Edholm, O. *Biophys. J.* **2011**, *100*, 2104.
- Pandey, A. P.; Haque, F.; Rochet, J. C.; Hovis, J. S. *Biophys. J.* **2009**, *96*, 540.
- Kjaer, L.; Giehm, L.; Heimborg, T.; Otzen, D. *Biophys. J.* **2009**, *96*, 2857.
- Mihajlovic, M.; Lazaridis, T. *Proteins* **2008**, *70*, 761.
- Braun, A. R.; Brandt, E. G.; Edholm, O.; Nagle, J. F.; Sachs, J. N. *Biophys. J.* **2011**, *100*, 2112.

- (53) Devaux, P. F.; Herrmann, A.; Ohlwein, N.; Kozlov, M. M. *Biochim. Biophys. Acta* **2008**, *1778*, 1591.
- (54) George, J. M.; Jin, H.; Woods, W. S.; Clayton, D. F. *Neuron* **1995**, *15*, 361.
- (55) Hellstrand, E.; Grey, M.; Ainalem, M.-L.; Ankner, J.; Forsyth, V. T.; Fragneto, G.; Haertlein, M.; Dauvergne, M.-T.; Nilsson, H.; Brundin, P.; Linse, S.; Nylander, T.; Sparr, E. *ACS Chem. Neurosci.* **2013**, *4*, 1339.
- (56) Lee, S. J. C.; Lee, J. W.; Choi, T. S.; Jin, K. S.; Lee, S.; Ban, C.; Kim, H. I. *Anal. Chem.* **2014**, *86*, 1909.
- (57) Ayton, G. S.; Lyman, E.; Krishna, V.; Swenson, R. D.; Mim, C.; Unger, V. M.; Voth, G. A. *Biophys. J.* **2009**, *97*, 1616.
- (58) Srivastava, A.; Voth, G. A. *J. Chem. Theory Comput.* **2013**, *9*, 750.
- (59) Ayton, G. S.; Lyman, E.; Voth, G. A. *Faraday Discuss.* **2010**, *144*, 347.
- (60) Ayton, G.; Voth, G. A. *Biophys. J.* **2002**, *83*, 3357.
- (61) Baoukina, S.; Tielemans, D. P. *Biophys. J.* **2010**, *99*, 2134.
- (62) Mim, C.; Unger, V. M. *Trends Biochem. Sci.* **2012**, *37*, 526.
- (63) Iyer, A.; Petersen, N. O.; Claessens, M. M. A. E.; Subramaniam, V. *Biophys. J.* **2014**, *106*, 2585.
- (64) Devaux, P. F. *Biochimie* **2000**, *82*, 497.
- (65) Anglin, T. C.; Brown, K. L.; Conboy, J. C. *J. Struct. Biol.* **2009**, *168*, 37.
- (66) Zhang, L.; Rozek, A.; Hancock, R. E. *J. Biol. Chem.* **2001**, *276*, 35714.
- (67) Perlmutter, J. D.; Sachs, J. N. *J. Am. Chem. Soc.* **2011**, *133*, 6563.
- (68) Mizuno, N.; Varkey, J.; Kegulian, N. C.; Hegde, B. G.; Cheng, N.; Langen, R.; Steven, A. C. *J. Biol. Chem.* **2012**, *287*, 29301.
- (69) Nakamura, K. *Neurotherapeutics* **2013**, *10*, 391.
- (70) Gaugler, M. N.; Genc, O.; Bobela, W.; Mohanna, S.; Ardah, M. T.; El-Agnaf, O. M.; Cantoni, M.; Bensadoun, J. C.; Schneggenburger, R.; Knott, G. W.; Aebsicher, P.; Schneider, B. L. *Acta Neuropathol.* **2012**, *123*, 653.
- (71) Auluck, P. K.; Caraveo, G.; Lindquist, S. *Annu. Rev. Cell Dev. Biol.* **2010**, *26*, 211.
- (72) Nemani, V. M.; Lu, W.; Berge, V.; Nakamura, K.; Onoa, B.; Lee, M. K.; Chaudhry, F. A.; Nicoll, R. A.; Edwards, R. H. *Neuron* **2010**, *65*, 66.
- (73) Zigoneanu, I. G.; Yang, Y. J.; Krois, A. S.; Haque, M. E.; Pielak, G. J. *Biochim. Biophys. Acta* **2012**, *1818*, 512.